

THE EFFECT OF AGN HEATING ON THE LOW-REDSHIFT LY α FORESTALEX GURVICH¹, BLAKESLEY BURKHART² & SIMEON BIRD³*Draft version February 8, 2017*

ABSTRACT

We investigate the effects of AGN heating and the ultraviolet background on the low-redshift Lyman- α forest column density distribution (CDD) using the Illustris simulation. We show that Illustris reproduces observations at $z = 0.1$ in the column density range $10^{12.5} - 10^{13.5} \text{ cm}^{-2}$, relevant for the “photon underproduction crisis.” We attribute this to the inclusion of AGN feedback, which changes the gas distribution so as to mimic the effect of extra photons, as well as the use of the Faucher-Giguère ultraviolet background, which is more ionizing at $z = 0.1$ than the Haardt & Madau background previously considered. We show that the difference between simulations run with smoothed particle hydrodynamics and simulations using a moving mesh is small in this column density range but can be more significant at larger column densities. We further consider the effect of supernova feedback, Voigt profile fitting and finite resolution, all of which we show to have little influence on the CDD. Finally, we identify a discrepancy between our simulations and observations at column densities $10^{14} - 10^{16} \text{ cm}^{-2}$, where Illustris produces too few absorbers, which suggests the AGN feedback model should be further refined. Since the “photon underproduction crisis” primarily affects lower column density systems, we conclude that AGN feedback and standard ionizing background models can resolve the crisis.

Subject headings: cosmology: theory – diffuse radiation – galaxies: formation – intergalactic medium – large-scale structure of universe

1. INTRODUCTION

Fifty years after Gunn & Peterson (1965) and Bahcall & Salpeter (1965) used quasar absorption systems to infer the neutral hydrogen density, the Lyman- α forest remains a key diagnostic of galaxy physics and cosmology. Lyman- α forest observations at $z \geq 2$, where the Lyman- α line can be observed from the ground, have been used to constrain the small-scale cosmic structure (Croft et al. 1998; McDonald et al. 2005), the temperature of dark matter (Viel et al. 2009), the gas temperature (Becker et al. 2011; Boera et al. 2014) and the evolution of the metagalactic ionizing background (Haardt & Madau 1996; Faucher-Giguère et al. 2008b,a, 2009; Haardt & Madau 2012). Meanwhile, observations of the abundance of stronger neutral hydrogen absorbers have been used as a test of cosmological structure models (e.g. Cen et al. 1994; Zhang et al. 1995; Hernquist et al. 1996; Miralda-Escudé et al. 1996; Rauch et al. 1997; Pontzen et al. 2008; Faucher-Giguère & Kereš 2011; Fumagalli et al. 2011, 2014; Bird et al. 2014; Faucher-Giguère et al. 2015, 2016). Studying the diffuse absorbing gas that produces the Lyman- α forest requires cosmological hydrodynamic simulations, which include both fully nonlinear gravitational collapse and the interaction between gravitational and photoionization heating and cooling processes.

Recent observations with the Hubble Space Telescope (*HST*; Lehner et al. 2007; Danforth et al. 2016) have en-

abled studies of the low-redshift Lyman- α forest. While at $z = 2$ the Lyman- α forest arises from an approximately mean density gas, by $z = 0$ it is a probe of gas closer to 10 times the cosmic mean (Davé et al. 1999). Thus, the low-redshift Lyman- α forest traces the diffuse gas in filaments and the outskirts of galaxies and clusters.

Importantly, photoionization equilibrium between the neutral hydrogen and the ionizing background provides a unique census of the number of ionizing photons at $z \approx 0$. In particular, Kollmeier et al. (2014, hereafter K14) reported a discrepancy of a factor of 3.3 between the observed column density distribution (CDD) data of (Danforth et al. 2016, D16), taken with the Cosmic Origins Spectrograph (COS) on HST, and the CDD derived using synthetic Lyman- α spectra from a simulation run with GADGET. They suggest that resolving this discrepancy requires increasing the number of ionizing photons at $z \approx 0$ by a factor of five over their fiducial (Haardt & Madau 2012, HM12) ultraviolet background (UVB) model. They consider this increase unlikely to be consistent with current observational uncertainties in the escape fraction of ionizing photons from galaxies. Thus, they suggest that resolving this “photon underproduction crisis” may require previously unobserved heating sources, such as blazars (Chang et al. 2012; Puchwein et al. 2012) or annihilating dark matter particles. Later work (Khaire & Srianand 2015) suggested that enough photons could be produced using updated models of quasar emissivity. Shull et al. (2015) suggested that the discrepancy could be resolved using only a factor of two increase in the ionization rate Γ_{HI} , a difference that they considered to be plausible.

Here, we re-examine this discrepancy in the context of the Illustris, a cosmological hydrodynamic simulation using the moving-mesh code AREPO, which includes a comprehensive model for the evolution of gas and galax-

¹ Department of Physics and Astronomy and CIERA, Northwestern University, 2145 Sheridan Road, Evanston, IL 60208, USA

agurvich@u.northwestern.edu

² Harvard-Smithsonian Center for Astrophysics, 60 Garden Street, Cambridge, MA 0213, USA

³ Department of Physics and Astronomy, Johns Hopkins University, 3400 N. Charles Street, Baltimore, MD 21218, USA

ies to $z = 0$, and has been shown to match several low-redshift properties of galaxies (e.g. Genel et al. 2014; Vogelsberger et al. 2014; Sijacki et al. 2015). We compare the CDD of neutral hydrogen in the Lyman- α forest from Illustris to the observations of D16. We investigate the effects of supernova and AGN feedback prescriptions, the hydrodynamic solver, the UVB model, and the method for estimating column densities. We find that the previously neglected effect of AGN feedback, together with a $1.7\times$ increase in the ionization rate over HM12 due a different UVB model from Faucher-Giguère et al. (2009), is sufficient to resolve the discrepancy at low column densities.

The paper is organized as follows. In Section 2, we introduce the simulations, in Section 3, we present the results of the comparison of the CDD from the simulations to the observations of D16. In Section 4, we discuss our results, followed by our conclusions in Section 5.

2. SIMULATIONS

We use the Illustris simulation (Genel et al. 2014; Vogelsberger et al. 2014; Nelson et al. 2015) to analyze the low-redshift Lyman- α forest CDD. Illustris is a cosmological hydrodynamic simulation in a box of length $75 h^{-1}\text{Mpc}$. Gravitational interactions from dark matter and baryons are evolved using the TreePM algorithm (Springel 2005). Radiative cooling is implemented using a rate network following Katz et al. (1996), including line cooling, free-free emission, and inverse Compton cooling. Illustris assumes ionization equilibrium and accounts for shielding from the radiation background at high hydrogen column densities, following Rahmati et al. (2013). Shielding is followed during the course of the hydrodynamic calculation and is thus included in the dynamics of the simulation. Metals and metal-line cooling are included as described in Vogelsberger et al. (2012). star-formation is implemented using the subgrid model of Springel & Hernquist (2003). The star-forming gas is assumed to have a temperature of $\sim 10^4\text{K}$ and is thus fully neutral for the purposes of HI absorption.

For hydrodynamics, Illustris uses the moving-mesh code AREPO (Springel 2010). Each grid cell on the moving mesh is sized to contain a roughly fixed amount of mass and to move approximately following the local bulk motion of the fluid. Small-scale mixing is included by allowing gas and metals to advect between grid cells. To assess the impact of the hydrodynamical solver on the CDD in Illustris, we examined two simulations from Vogelsberger et al. (2012). While these simulations were designed to have identical initial conditions and gravitational evolution, they used different codes with different hydrodynamical solvers. One used AREPO, while the other used the smoothed particle hydrodynamics (SPH) code GADGET-3 (Springel 2005). Neither of these simulations include feedback, allowing a clean comparison between numerical hydrodynamical methods without being affected by implementation differences in the star-formation/AGN models.

The ultraviolet background (UVB) in Illustris follows the estimates of Faucher-Giguère (2009, henceforth FG09). K14 used the UVB model of HM12. Both UVB models are calibrated primarily at $z = 2 - 4$, but the FG09 UVB has a shallower slope at lower redshift, so that by $z \sim 0$ it produces about 1.7 times more ionizing

photons, differing from HM12 by $\Delta\Gamma_{\text{HI}} = 1.6 \times 10^{-14} \text{ s}^{-1}$. To confirm the magnitude of this effect on the CDD, we have performed a simulation using the Illustris fiducial setup, but with an HM12 UVB.

As described in detail in Vogelsberger et al. (2013), Illustris includes phenomenological models for stellar and AGN feedback that aims to capture the unresolved influence of these energetic events on their environment. The parameters of these feedback models have been adjusted to approximately reproduce the galactic stellar mass function and star-formation rates at $z = 0$ by suppressing star-formation relative to pure gravitational collapse. In general, the supernova feedback model dominates in low-mass objects, while the AGN feedback is effective in high-mass systems.

The supernova feedback model suppresses star-formation via kinetic feedback from star-forming cells to nearby gas cells. The total energy of the supernova wind is held constant and is given by

$$\text{egy}_w = \frac{1}{2}\eta_w v_w^2, \quad (1)$$

where η_w is the wind mass loading and v_w is the wind velocity. v_w scales with the local dark matter velocity dispersion, which correlates with the maximum dark matter circular velocity of the host halo (Oppenheimer & Davé 2008). The Illustris wind model thus yields large mass loadings in small halos (as egy_w is constant), which allows it to roughly match the galaxy stellar mass function at $z = 0$ (Okamoto et al. 2010; Puchwein & Springel 2013). The parameters of the wind model are described in detail in Vogelsberger et al. (2013).

As implemented in Illustris, AGN feedback suppresses star-formation in the most massive halos by periodically releasing thermal energy from the black hole into the gas cells surrounding it (Di Matteo et al. 2005; Springel et al. 2005; Sijacki et al. 2007; Vogelsberger et al. 2013). The AGN feedback model has two modes: quasar-mode feedback and radio-mode feedback. Quasar-mode feedback is in operation when the central black hole of the halo has high accretion rates. Here, a small fraction of the rest-mass energy of the accreted material couples directly to the dense gas surrounding the black hole. Radio-mode feedback, which operates at low accretion rates, is implemented by the formation of thermal bubbles in the gas around the black hole. This feedback mode significantly decreases the star-formation rate in massive halos (Vogelsberger et al. 2013) and substantially reduces the gas density up to $\sim 1 \text{ Mpc}$ from the host halo (van Daalen et al. 2011; Sijacki et al. 2015). Illustris also includes the local effect of radiation from the central quasar, although this is only important for accretion rates close to the Eddington limit. Weinberger et al. (2016) suggested an updated model for accretion and feedback effects of AGN to ameliorate several known discrepancies between observed and simulated galaxy properties in the Illustris simulation, such as the low gas fraction in groups of galaxies and clusters. Here, we investigate the Lyman- α forest using the fiducial Illustris feedback model (Vogelsberger et al. 2013) and will explore the effects of the updated prescription of Weinberger et al. (2016) in a future work.

Illustris initially contains 1820^3 dark matter particles

and 1820^3 gas elements. To check the convergence of our results with respect to the box size and resolution, and to investigate the impact of different feedback models and hydrodynamical solvers, we used several smaller simulations, all with a box size of $25 h^{-1}\text{Mpc}$. The simulations varying the hydrodynamical solver and UVB amplitude have 2×512^3 particles, giving a resolution approximately equal to Illustris, while the simulations varying the feedback model have 2×256^3 particles. We summarize the basic setup of all simulations used in this study and provide their parameters in Table 1.

2.1. Analysis

We define the CDD function, $f(N_{\text{HI}})$, by

$$f(N_{\text{HI}}) = \frac{F(N)}{\Delta N} \Delta z. \quad (2)$$

$F(N)$ is the number of absorbers per sightline with column density in the interval $[N_{\text{HI}}, N_{\text{HI}} + dN_{\text{HI}}]$, over the redshift interval Δz contained in our simulated spectra. We estimate the CDD from the column density along 25,000 simulated skewers randomly positioned in each simulation box. Column densities are computed by interpolating the neutral hydrogen in each gas element to the sightline using an SPH kernel. A single absorber is 50 km s^{-1} across, although we have checked that our results are not sensitive to this value. Thus, our column densities correspond to the integrated physical density field in the simulation and provide a quick and scalable way to examine the physical state of the absorber. The procedure is described in detail in Bird et al. (2015) and the implementation is available at https://github.com/sbird/fake_spectra.

We also investigated estimating column densities by Voigt fitting to the optical depth along our simulated spectra. We describe our procedure in Appendix B and show that the method used makes a negligible difference to our results. Following K14 we perform Voigt fitting using AUTOVP (Oppenheimer & Davé 2006).

3. RESULTS

Figure 1 shows our main result, the $z = 0.1$ HI CDD from the Illustris simulation compared to the numerical results of K14 and observations of D16. Illustris reproduces the amplitude of the observed CDD at low column densities without the offset seen by K14. However, Illustris does not reproduce the shape of the CDD at higher column densities, $N_{\text{HI}} > 10^{13.5} \text{ cm}^{-2}$, producing too few absorbers. In the rest of this section, we discuss why Illustris reproduces the observed CDD amplitude at low column densities, while leaving the discrepancy in the shape at higher column densities for Section 4.

The observational survey of D16 includes absorbers for $z = 0.1 - 0.47$. While we report results at $z = 0.1$, near the median redshift of the survey, we have checked that the CDD is very similar if we average simulation outputs over the observed range of redshifts. For easy comparison with K14, we show the column density range used in that work, but in future plots we also show larger column densities, as the observational survey of D16 includes these absorbers.

3.1. Effect of the Hydrodynamic Solver

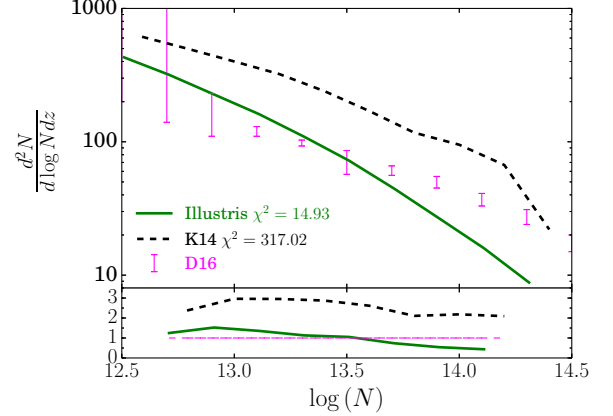


FIG. 1.— CDD from Illustris $75 h^{-1}\text{Mpc}$ at $z = 0.1$ (green solid), compared to the simulations of K14 (Kollmeier et al. 2014, black dashed) and the observations of D16 (Danforth et al. 2016, magenta points). The lower panel shows the ratio of each simulation with the D16 results. The column density range is chosen to match that shown by K14. Illustris reproduces the amplitude of the observed CDD well, without the offset seen by K14. However, Illustris does not reproduce the shape of the CDD at higher column densities, $N_{\text{HI}} > 10^{13.5} \text{ cm}^{-2}$, producing too few absorbers.

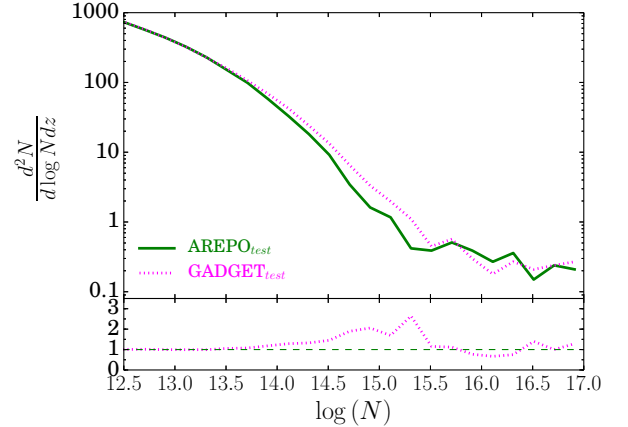


FIG. 2.— Effect of the hydrodynamic solver on the column density distribution at $z = 0$ using smoothed particle hydrodynamics (GADGET, magenta dashed) and an otherwise identical simulation performed using a moving-mesh (AREPO, green solid). The lower panel shows the GADGET simulation divided by the AREPO simulation. There is not a significant difference between the two codes at the low column density range studied in K14.

One possible reason for the discrepancy between our results and the simulations of K14 is the hydrodynamic solver used. Illustris uses the code AREPO with a moving-mesh solver for hydrodynamics, while the simulations analyzed in K14 use GADGET with smoothed particle hydrodynamics. Figure 2 shows results from the $z = 0$ output of two simulations from Vogelsberger et al. (2012) designed specifically to assess the effect of the hydrodynamic solver. These simulations have identical initial conditions and gravity solvers, but different hydrodynamic methods.

For column densities $10^{14} < N_{\text{HI}} < 10^{15.5} \text{ cm}^{-2}$, AREPO produces about half as many absorbers as GADGET. As shown in Bird et al. (2013), GADGET overpredicts the number of 10^{17} cm^{-2} absorbers at

TABLE 1
DESCRIPTION OF SIMULATIONS

Name	AGN Feedback?	ϵ_m^a	SNe Feedback?	UVB Model used	Box Size	Particles	Reference	Figures
Illustris	Yes	0.35	Yes	FG09	$75 h^{-1} \text{Mpc}$	1820^3	V14 ^b	1,7,A
Illustris-small	Yes	0.35	Yes	FG09	$25 h^{-1} \text{Mpc}$	512^3	V13 ^c	3,7
Illustris-lowres	Yes	0.35	Yes	FG09	$25 h^{-1} \text{Mpc}$	256^3	V13	5,4,7
Stellar	No	...	Yes	FG09	$25 h^{-1} \text{Mpc}$	256^3	V13	4
No Feedback	No	...	No	FG09	$25 h^{-1} \text{Mpc}$	256^3	V13	4,5
Stronger Radio	Yes	0.7	Yes	FG09	$25 h^{-1} \text{Mpc}$	256^3	V13	5
Weaker Radio	Yes	0.175	Yes	FG09	$25 h^{-1} \text{Mpc}$	256^3	V13	5
HM12 _{AREPO}	Yes	0.35	Yes	HM12	$25 h^{-1} \text{Mpc}$	512^3	...	3
AREPO _{test}	No	...	No	FG09	$25 h^{-1} \text{Mpc}$	512^3	V12 ^d	2
Gadget _{test}	No	...	No	FG09	$25 h^{-1} \text{Mpc}$	512^3	V12	2

^a ϵ_m is the AGN feedback radio-mode energy fraction. See Table 1 of Vogelsberger et al. (2013).

^bVogelsberger et al. (2014)

^cVogelsberger et al. (2013)

^dVogelsberger et al. (2012)

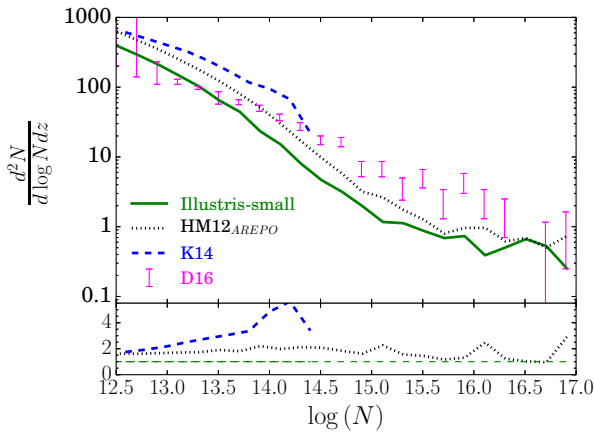


FIG. 3.— Impact of changing the ultraviolet background (UVB) on the CDD at $z = 0.1$. The Illustris-small simulation, which uses the FG09 UVB, is indicated in green (solid), while an identical simulation using the HM12 UVB is shown in black (dotted). The lower panel shows the ratio of each curve to the Illustris-small results. The different UVBs used account for about half of the difference between the CDD in Illustris and the CDD of K14 (as shown with the HM12_{AREPO} simulation).

$z = 3$ by a factor of two, and here we see the low-redshift analogue of that discrepancy. Note that the column density 10^{15} cm^{-2} at $z \sim 0$ probes a similar physical density to a column density of 10^{17} cm^{-2} at $z \sim 3$ (Davé et al. 1999). However, the difference between D16 and K14 is confined to column densities $N_{\text{HI}} < 10^{14} \text{ cm}^{-2}$, and thus the hydrodynamic solver cannot account for the differences in that range.

3.2. The UVB

Figure 3 shows the effect of changing the UVB on two AREPO simulations using the Illustris feedback model. We compare the FG09 UVB, the default in Illustris, to the HM12 UVB used by K14. Both UVB models are calibrated primarily at $z = 2 - 4$, but the FG09 UVB decreases less strongly at lower redshifts, so that by $z \sim 0$ it produces 1.7 times more ionizing photons. As discussed by K14, at $z \sim 0.1$ these column densities probe gas that is both highly ionized and in photoionization equilibrium. Thus, $N_{\text{HI}} \propto 1/\Gamma_{\text{HI}}$, so that the effect of changing the UVB from HM12 to FG09 is to decrease column den-

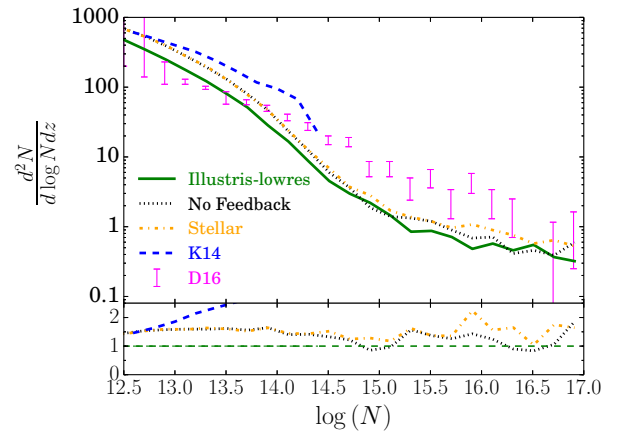


FIG. 4.— Effect of feedback models on the $z = 0.1$ CDD: the Illustris-lowres 25 Mpc simulation at $z = 0.1$, which includes both stellar and AGN feedback, is indicated in green (solid). A simulation with neither AGN nor supernova feedback is indicated with a black (dotted) line, while a similar model without AGN feedback but with supernova feedback is shown in blue (dot-dashed) and labeled “Stellar.” The lower panel shows the ratio of each CDD to the Illustris-lowres simulation. The supernova feedback has negligible effect on the CDD for column densities $N_{\text{HI}} < 10^{16} \text{ cm}^{-2}$.

ties by 1.7. In practice, the effect is slightly larger than expected; the FG09 simulation is a good match to the HM12 simulation when column densities are divided by a factor of 1.9, reflecting second-order terms in the photoionization equilibrium. Thus, the different UVBs used account for about half of the difference between the CDD in Illustris/D16 and the CDD of K14.

3.3. The Effects of Feedback

Figure 4 shows the effect of the supernova feedback models used. We show a simulation with no feedback, one with supernova feedback only, and finally the Illustris-lowres simulation, which includes both stellar and AGN feedback. The supernova feedback has a negligible effect on the CDD for column densities $N_{\text{HI}} < 10^{16} \text{ cm}^{-2}$. This is not surprising. Supernova feedback changes the distribution of the gas only in regions relatively close to star-forming halos, while the CDD at this column density probes gas up to a few megaparsecs from galaxies (Davé et al. 1999; Shull et al. 2015). The simulations of K14 include supernova feed-

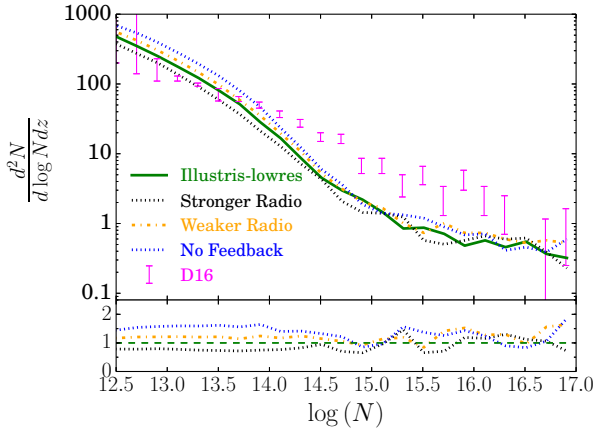


FIG. 5.— Effect of changing the strength of the AGN feedback from Illustris-lowres simulation (green solid line) with stronger (black dotted line) or weaker (orange dot-dashed line) radio-mode prescriptions along with the no feedback case for reference. The lower panel shows the ratio of each simulation column density distribution to the Illustris-lowres simulation.

back but not AGN feedback. The “vzw” feedback model (Oppenheimer & Davé 2008) used in K14 is similar to ours but with parameters that make it somewhat more efficient at expelling gas from large halos. Their results are thus most closely comparable to our orange “Stellar” curve in Figure 4, with column densities multiplied by a factor of 1.9 to account for the differing UVBs.

The AGN feedback (included in the Illustris simulation shown with a green line) suppresses the HI CDD at column densities $N_{\text{HI}} = 10^{12.5} - 10^{14.5} \text{ cm}^{-2}$ by a factor of 1.5 with respect to the no feedback case. This occurs not because of a change in the photoionization equilibrium⁴, but because the AGN both reduces the gas density at distances of ~ 1 Mpc or more from galaxies and heats the remaining gas. Both of these effects conspire to reduce the neutral gas density (Sijacki et al. 2015; Suresh et al. 2015). Figure 5 shows the sensitivity of this effect to the strength of the AGN feedback. Here we alter the fraction of the AGN accretion energy, which couples to the gas via the radio mode (effective at suppressing star-formation). Changing this tunable parameter by a factor of two with respect to the default setting used in Illustris changes the CDD by about 30%, Genel et al. (2014) showed that the Illustris AGN feedback model is too strong as it over-suppresses the gas fraction in massive halos. However, the fact that varying the AGN feedback alters the CDD suggests that AGN feedback models could now be tuned using the Lyman- α Forest. We therefore conclude that AGN feedback can have a significant effect on the CDD at low redshifts and discuss the implications of this further in Section 4.

4. DISCUSSION

4.1. Is there a “Photon Underproduction Crisis?”

Recent studies have found that the UVB Γ_{HI} model of Haardt & Madau (2012) is not consistent with the low-redshift CDD. In particular, the predicted $z = 0$ Γ_{HI} from Haardt & Madau (2012) is five times lower than

⁴ While the local radiation effects of the AGN are included, they are not large enough.

required by the simulations of K14 and three times lower than required by Shull et al. (2015). This has led to the suggestion of a “photon underproduction crisis” for the low redshift Lyman- α forest. K14 provided a detailed discussion of possible resolutions to the crisis, including boosting the quasar emissivity, the galaxy escape fraction, extra heating sources, altering the mean free path of ionizing photons, as well as considering new sources of ionizing photons.

In this work, we investigate the effects of altering aspects of cosmological simulations including the feedback prescription, Γ_{HI} , and the hydrodynamic solver. We find that the main drivers, in our analysis, of the discrepancy between the D16 observational data and simulations are the absence of AGN feedback and the cosmic UV background model adopted for Γ_{HI} . AGN feedback was not included in the GADGET simulations presented in K14. We find that the inclusion of AGN feedback can substantially alter the CDD at the low column densities studied here. This is because strong radio AGN feedback can substantially heat and ionize the gas, even more than 1 Mpc from the halo (Zhu et al. 2016), which will reduce the neutral column density. In the Illustris model, radio-mode AGN feedback leads to significant gas heating at $z < 2$, especially in more massive halos, where it is the main regulator of star-formation (see Vogelsberger et al. 2014). This is shown visually in Figure 6, where we plot the HI column density integrated in 1.5 Mpc around the largest halo in our Illustris-small and Stellar simulations, which differ only in the presence of AGN feedback. AGN reduce HI densities, especially for the column ranges observed by Danforth et al. (2016). Stronger columns appear to be less affected, likely because higher density absorbers are harder to disrupt. Our study is complimentary to those of Shull et al. (2015), Khaire & Srianand (2015), and Gaikwad et al. (2016), who showed that updated QSO and galaxy emissivity properties were sufficient to increase Γ_{HI} by a factor of ≈ 2 and could increase Γ_{HI} by a factor of five with larger galaxy photon escape fractions. While this suffices to produce enough photons, we show that with the addition of AGN feedback only a factor two increase in photon production is necessary, which is achieved, within current observational uncertainties, by using the FG09 model. Therefore, with AGN feedback and the FG09 UVB, Illustris is able to better match the D16 observations for $N_{\text{HI}} = 10^{12.5} - 10^{13.5} \text{ cm}^{-2}$ and the “photon underproduction crisis” can be fully resolved.

4.2. The AGN Feedback Model in Illustris and Higher Column Densities

As shown in Genel et al. (2014), the Illustris AGN feedback model over-suppresses the gas fraction in massive halos, indicating that the feedback model is overly effective at expelling gas from the halo. However, this problem is unlikely to affect the results we present for $N_{\text{HI}} = 10^{12.5} - 10^{14} \text{ cm}^{-2}$. These absorbers correspond to baryon over-densities in the range 4 – 40 (Shull et al. 2015) and are thus around 2Mpc from the halo. For comparison, the halos in which the gas fraction is over-suppressed have masses $10^{13} - 10^{14} M_{\odot}$ and virial radii $R_{500} = 300 - 700 \text{ kpc}$. They also comprise a small fraction of the total volume of the simulation, which is dominated by smaller halos. Furthermore, a sup-

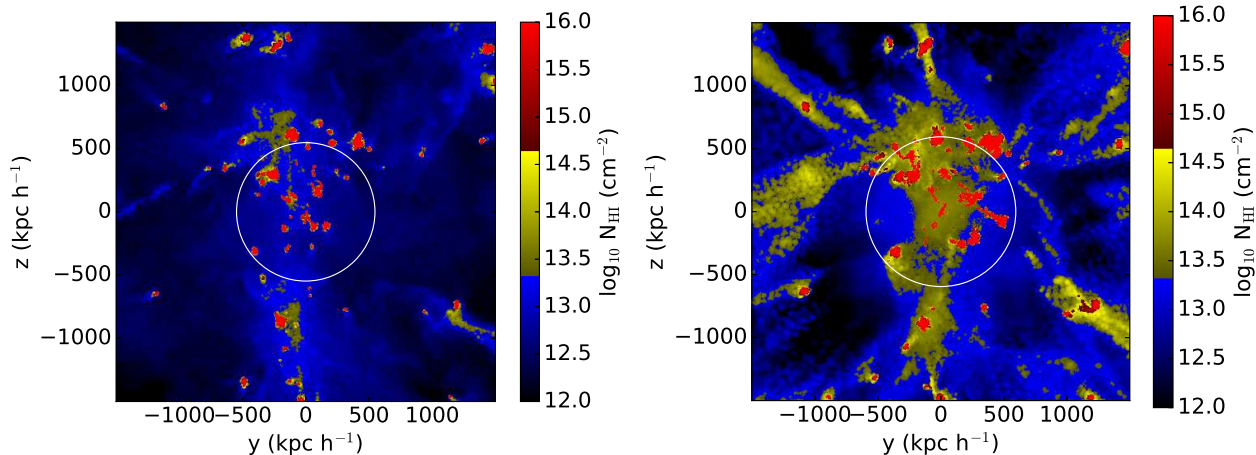


FIG. 6.— HI column density integrated over a 1.5Mpc slice in a 1.5Mpc box around the largest halo in our Illustris-small and Stellar simulations. (Left) Illustris-small simulation, which includes AGN and stellar feedback. (Right) Stellar simulation, which does not include AGN feedback. The AGN feedback substantially reduces the HI column density up to 1.5Mpc from the halo.

pression of neutral gas at megaparsec distances from the halo is a generic feature of AGN feedback models (van Daalen et al. 2011). Overall, then, our principle result that AGN feedback is a significant factor in reconciling simulations with the D16 observations at low column densities seems robust to modest changes in the underlying model.

There is a discrepancy between the COS observations and our AREPO simulations at $10^{13.5} < N_{\text{HI}} < 10^{15.5} \text{ cm}^{-2}$. In this column density range, Illustris produces a factor of two too few absorbers. These stronger columns are associated with denser regions closer to the halos, where the over-vigorous expulsion of gas in the Illustris AGN feedback model may have a larger impact. There may thus be sufficient freedom in the model to resolve the disagreement between observations and simulations. This would not be the only example of a discrepancy between observations and Illustris resulting from the AGN feedback model. For example, in the Illustris simulation the stellar masses of the central galaxies in the simulated systems are also too high as a result of the overactive AGN feedback model. Future studies will investigate the low-redshift Lyman- α forest CDD using an updated model for AGN feedback (Weinberger et al. 2016) in order to investigate the number of absorbers at medium column densities.

We note, however, that our models with no feedback and supernova feedback also underproduce absorbers in the column density range $10^{14} < N_{\text{HI}} < 10^{15.5} \text{ cm}^{-2}$. K14 simulations do not suffer from this discrepancy, but their simulations did not include the effect of self-shielding, which may start to become important for these column densities. Interestingly, the simulations of Shull et al. (2015) also underproduce stronger systems in their preferred model. This suggests that the full solution may be more involved.

For example, in the flat ($N_{\text{HI}} = 10^{14} - 10^{18} \text{ cm}^{-2}$) regime of the curve of growth (CoG), the HI equivalent width depends strongly on both the column density of the absorber and the kinematic and thermal state of the gas (i.e. the Doppler broadening of the line). Thus, the CDD could potentially be affected by turbulent broadening, which is unresolved in numerical simulations. Indeed, most turbulence box simulations require grid reso-

lutions of at least 512^3 before resolving the inertial range cascade (Burkhart et al. 2009). Cosmological numerical simulations do not have the spatial resolution to resolve turbulence in the IGM and this is especially true of simulations that set the spatial refinement based on quasi-Lagrangian refinement, which puts most of the spatial resolution inside galaxies. Therefore, the IGM in Illustris, which has the poorest spatial resolution sampling because it consists of the lowest density environments, cannot resolve all of the kinematic motions that may be present in the observations. The effects of turbulence on the IGM statistics, including the Lyman- α CDD, in the linear regime of the CoG will be closely examined in a future work.

We found that the CDD in this column density range was also affected by the hydrodynamic solver used. SPH simulations can suppress turbulence and mixing, which can affect thermal conduction (Biffi & Valdarnini 2015) galaxy formation (Keres et al. 2011) in idealized test cases (Sijacki et al. 2012). While the differences between AREPO and GADGET were small at lower column densities, they were a factor of two for $10^{14} < N_{\text{HI}} < 10^{15.5} \text{ cm}^{-2}$. This mirrors the results of Bird et al. (2013), who found that SPH tends to produce spurious clumps in gas at this physical density. Any future simulation work on this discrepancy should use a hydrodynamical solver that is sufficiently accurate in this regime.

5. CONCLUSION

We examined the $z = 0.1$ CDD in the Illustris simulation. We find that the Illustris simulation matches the D16 observations for the column density range of $N_{\text{HI}} = 10^{12.5} - 10^{13.5} \text{ cm}^{-2}$ significantly better than previous work for the same photoionization rate as a result of the inclusion of AGN feedback. We investigated the effects on our results of the hydrodynamic solver, supernova, and AGN feedback models, as well as the UVB model. We found that the most significant factors affecting agreement with observations were the UVB model and the inclusion of AGN feedback (radio mode, quasar mode, and radiative). The Faucher-Giguère et al. (2009) UVB model we used, in conjunction with the inclusion of AGN feedback, matches current observations at low redshifts at a better level than Kollmeier et al. (2014) sim-

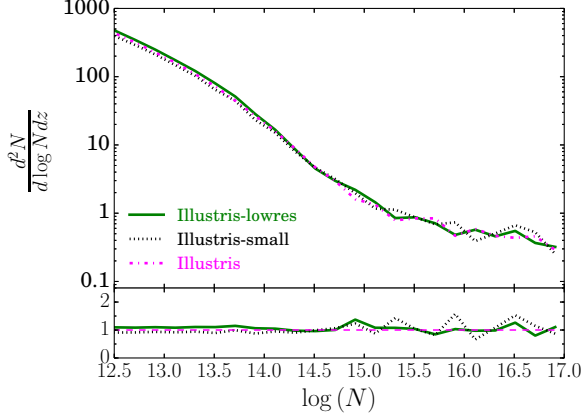


FIG. 7.— HI CDD as measured using the direct method at $z = 0.1$ from the full Illustris simulation (magenta dot-dashed), with a 75 Mpc box and 1820^3 particles, compared to Illustris-small (black dotted), a 25 Mpc box with 512^3 particles. Also shown is Illustris-lowres (green solid), a 25 Mpc box with 256^3 particles. The lower panel shows the ratio of each simulation to Illustris.

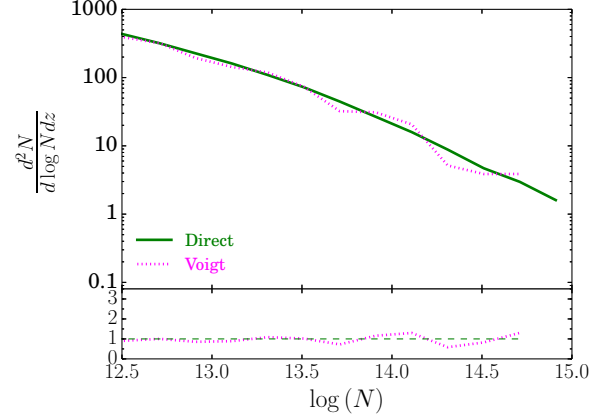


FIG. 8.— Column density function from Illustris 75 Mpc at $z = 0.1$, estimated using both direct summation of column densities (green solid) and using Voigt profile fitting (magenta dotted). The lower panel shows the ratio of the Voigt fitted CDD to the direct summation estimate.

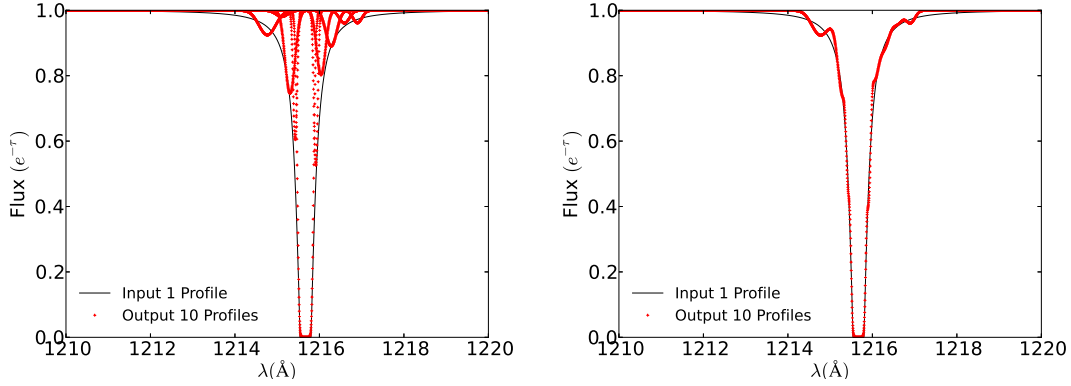


FIG. 9.— (Left) Idealized Voigt profile (black) with $b = 10 \text{ km s}^{-1}$ and $N = 10^{18} \text{ cm}^{-2}$ with the output parameters of the fit Voigt profiles from AUTOVP stacked on top (red). (Right) Same Voigt profile (black) overlaid with the sum of the fitted output profiles (red).

ulations that used the UVB of Haardt & Madau (2012) and no AGN feedback. However, in contrast to the situation at $z > 2$, our simulations underproduce absorbers at column densities $N_{\text{HI}} > 10^{13.5} \text{ cm}^{-2}$, which may indicate a need to modify feedback models.

We showed that AGN feedback can significantly suppress the column density function in the range of $N_{\text{HI}} = 10^{12.5} - 10^{14.5} \text{ cm}^{-2}$. The effect of AGN feedback has not formerly been addressed and so our work demonstrates a new potential solution to the “photon underproduc-

tion crisis.” While the AGN feedback model in Illustris needs to be refined, our results suggest that AGN feedback can significantly affect these column densities, and thus must be considered in any future work on the HI CDD. The measurements of Danforth et al. (2016) may constitute the first observational evidence for the effect of AGN feedback on neutral gas around galactic halos and could provide an additional diagnostic to tune AGN feedback models in simulations.

APPENDIX

NUMERICAL CONVERGENCE

Figure 7 shows a convergence test of our simulations, examining both resolution and box size. We compare the full $75 h^{-1} \text{ Mpc}$ Illustris box with 1820^3 particles to identical simulations in a $25 h^{-1} \text{ Mpc}$ box. The first simulation (Illustris-small) has 2×512^3 resolution elements, and thus identical spatial resolution to Illustris, in a smaller box. The second simulation (Illustris-lowres) has 2×256^3 resolution elements, and thus a factor of two lower spatial resolution. Differences between the CDDs in the column density range of interest are negligible and due mostly to sample variance, demonstrating that our results are insensitive to changes in both the box size and the resolution.

VOIGT FITTING

We have estimated the CDD using two separate methods. The first, which is used for all figures in the main section of the paper, we call direct summation. The column density here is estimated via the integral of the density field in 50 km s^{-1} along a sightline. The bins exclude peculiar velocities and reflect the Hubble flow. The CDD function is computed via a histogram of the column densities. This column density estimator has the advantage of being extremely quick and scalable. However, it differs from the practice of observers, who use Voigt profile fitting to estimate the column density from optical depth spectra.

In this appendix, we will estimate the CDD using automated Voigt fitting as a check that this difference does not affect our results. First, artificial spectra are generated from each particle. Each particle is redshifted according to its peculiar velocity and the optical depth is generated by convolving a Voigt profile with the SPH kernel. Thermal broadening is included using the temperature of the particle. We then estimate the column density that would be observed using an automated Voigt profile fitter on these simulated spectra. Following Kollmeier et al. (2014), we used primarily AUTOVP⁵ (Davé et al. 1997). AUTOVP is a fully automated Voigt fitter that fits the profiles after adding simulated noise. Each line is subtracted in turn until the remaining features are consistent with the noise in the spectrum. A global re-fit of the lines is then performed. We used the default AUTOVP parameters and verified that our results were independent of adjusting these values.

Figure A shows the CDD estimated from both Voigt fitting and direct summation. They are in extremely good agreement. The resulting minor discrepancies are consistent with variance due to the added noise in the Voigt spectra. Note that due to the increased computational cost of Voigt fitting, Figure A is estimated using only 5000 sightlines. This validates our decision to use direct summation for the main results in our paper.

Figure A does not include results for column densities $N_{\text{HI}} > 10^{15} \text{ cm}^{-2}$. In this partially saturated regime we were unable to reliably fit the profiles with the publicly available version of AUTOVP. Figure 9 shows an example of this problem on an idealized test case. While the overall fit to the profile is visually reasonable, AUTOVP is arbitrarily fitting the high column density absorber with multiple lower column density systems. Fortunately, high column density systems are rare, and thus this problem does not substantially impact lower column density absorbers. We have verified this point using our own parallel Voigt fitter implemented in Python⁶, which we verified is able to correctly fit high column density systems. The resulting CDD still matches that estimated by direct summation, including at column densities up to 10^{17} cm^{-2} .

The authors are grateful for many valuable discussions with Lars Hernquist. The authors also thank the anonymous reviewer and Claude-André Faucher-Giguère for their very helpful suggestions. A.G. acknowledges support from the NSF REU program through grant Number 1262851. B.B. acknowledges support from the NASA Einstein Postdoctoral Fellowship. S.B. was supported by NASA through Einstein Postdoctoral Fellowship Award Number PF5-160133.

REFERENCES

- Bahcall, J. N., & Salpeter, E. E. 1965, *ApJ*, 142, 1677
- Becker, G. D., Bolton, J. S., Haehnelt, M. G., & Sargent, W. L. W. 2011, *MNRAS*, 410, 1096
- Biffi, V., & Valdarnini, R. 2015, *MNRAS*, 446, 2802
- Bird, S., Haehnelt, M., Neeleman, M., et al. 2015, *MNRAS*, 447, 1834
- Bird, S., Vogelsberger, M., Haehnelt, M., et al. 2014, *MNRAS*, 445, 2313
- Bird, S., Vogelsberger, M., Sijacki, D., et al. 2013, *MNRAS*, 429, 3341
- Boera, E., Murphy, M. T., Becker, G. D., & Bolton, J. S. 2014, *MNRAS*, 441, 1916
- Burkhart, B., Falceta-Gonçalves, D., Kowal, G., & Lazarian, A. 2009, *ApJ*, 693, 250
- Cen, R., Miralda-Escudé, J., Ostriker, J. P., & Rauch, M. 1994, *ApJ*, 437, L9
- Chang, P., Broderick, A. E., & Pfrommer, C. 2012, *ApJ*, 752, 23
- Croft, R. A. C., Weinberg, D. H., Katz, N., & Hernquist, L. 1998, *ApJ*, 495, 44
- Danforth, C. W., Keeney, B. A., Tilton, E. M., et al. 2016, *ApJ*, 817, 111
- Davé, R., Hernquist, L., Katz, N., & Weinberg, D. H. 1999, *ApJ*, 511, 521
- Davé, R., Hernquist, L., Weinberg, D. H., & Katz, N. 1997, *ApJ*, 477, 21
- Di Matteo, T., Springel, V., & Hernquist, L. 2005, *Nature*, 433, 604
- Faucher-Giguère, C.-A., Feldmann, R., Quataert, E., et al. 2016, *MNRAS*, 461, L32
- Faucher-Giguère, C.-A., Hopkins, P. F., Kereš, D., et al. 2015, *MNRAS*, 449, 987
- Faucher-Giguère, C.-A., & Kereš, D. 2011, *MNRAS*, 412, L118
- Faucher-Giguère, C.-A., Lidz, A., Hernquist, L., & Zaldarriaga, M. 2008a, *ApJ*, 688, 85
- Faucher-Giguère, C.-A., Lidz, A., Zaldarriaga, M., & Hernquist, L. 2009, *ApJ*, 703, 1416
- Faucher-Giguère, C.-A., Prochaska, J. X., Lidz, A., Hernquist, L., & Zaldarriaga, M. 2008b, *ApJ*, 681, 831
- Fumagalli, M., O’Meara, J. M., Prochaska, J. X., Kanekar, N., & Wolfe, A. M. 2014, *MNRAS*, 444, 1282
- Fumagalli, M., Prochaska, J. X., Kasen, D., et al. 2011, *MNRAS*, 418, 1796
- Gaikwad, P., Khaire, V., Choudhury, T. R., & Srianand, R. 2016, *ArXiv e-prints*, arXiv:1605.02738
- Genel, S., Vogelsberger, M., Springel, V., et al. 2014, *MNRAS*, 445, 175
- Gunn, J. E., & Peterson, B. A. 1965, *ApJ*, 142, 1633
- Haardt, F., & Madau, P. 1996, *ApJ*, 461, 20
- . 2012, *ApJ*, 746, 125
- Hernquist, L., Katz, N., Weinberg, D. H., & Miralda-Escudé, J. 1996, *ApJ*, 457, L51
- Katz, N., Weinberg, D. H., & Hernquist, L. 1996, *ApJS*, 105, 19
- Keres, D., Vogelsberger, M., Sijacki, D., Springel, V., & Hernquist, L. 2011, *ArXiv e-prints*, arXiv:1109.4638
- Khaire, V., & Srianand, R. 2015, *MNRAS*, 451, L30
- Kollmeier, J. A., Weinberg, D. H., Oppenheimer, B. D., et al. 2014, *ApJ*, 789, L32
- Lehner, N., Savage, B. D., Richter, P., et al. 2007, *ApJ*, 658, 680
- McDonald, P., Seljak, U., Cen, R., et al. 2005, *ApJ*, 635, 761
- Miralda-Escudé, J., Cen, R., Ostriker, J. P., & Rauch, M. 1996, *ApJ*, 471, 582
- Nelson, D., Pillepich, A., Genel, S., et al. 2015, *Astronomy and Computing*, 13, 12
- Okamoto, T., Frenk, C. S., Jenkins, A., & Theuns, T. 2010, *MNRAS*, 406, 208
- Oppenheimer, B. D., & Davé, R. 2006, *MNRAS*, 373, 1265
- . 2008, *MNRAS*, 387, 577

⁵ https://bitbucket.org/benopp/autovp_phys

⁶ https://github.com/sbird/fake_spectra/voigtfit.py

- Pontzen, A., Governato, F., Pettini, M., et al. 2008, MNRAS, 390, 1349
- Puchwein, E., Pfrommer, C., Springel, V., Broderick, A. E., & Chang, P. 2012, MNRAS, 423, 149
- Puchwein, E., & Springel, V. 2013, MNRAS, 428, 2966
- Rahmati, A., Pawlik, A. H., Raicevic, M., & Schaye, J. 2013, MNRAS, 430, 2427
- Rauch, M., Miralda-Escudé, J., Sargent, W. L. W., et al. 1997, ApJ, 489, 7
- Shull, J. M., Moloney, J., Danforth, C. W., & Tilton, E. M. 2015, ApJ, 811, 3
- Sijacki, D., Springel, V., Di Matteo, T., & Hernquist, L. 2007, MNRAS, 380, 877
- Sijacki, D., Vogelsberger, M., Genel, S., et al. 2015, MNRAS, 452, 575
- Sijacki, D., Vogelsberger, M., Kereš, D., Springel, V., & Hernquist, L. 2012, MNRAS, 424, 2999
- Springel, V. 2005, MNRAS, 364, 1105
- . 2010, MNRAS, 401, 791
- Springel, V., Di Matteo, T., & Hernquist, L. 2005, MNRAS, 361, 776
- Springel, V., & Hernquist, L. 2003, MNRAS, 339, 289
- Suresh, J., Bird, S., Vogelsberger, M., et al. 2015, MNRAS, 448, 895
- van Daalen, M. P., Schaye, J., Booth, C. M., & Dalla Vecchia, C. 2011, MNRAS, 415, 3649
- Viel, M., Bolton, J. S., & Haehnelt, M. G. 2009, MNRAS, 399, L39
- Vogelsberger, M., Genel, S., Sijacki, D., et al. 2013, MNRAS, 436, 3031
- Vogelsberger, M., Sijacki, D., Kereš, D., Springel, V., & Hernquist, L. 2012, MNRAS, 425, 3024
- Vogelsberger, M., Genel, S., Springel, V., et al. 2014, Nature, 509, 177
- Weinberger, R., Springel, V., Hernquist, L., et al. 2016, MNRAS, 00, 000
- Zhang, Y., Anninos, P., & Norman, M. L. 1995, ApJ, 453, L57
- Zhu, Z., Xu, H., Wang, J., et al. 2016, ApJ, 816, 54